ISSN 2616-5880 Vol. 7, Issue 1: 64-72, DOI: 10.25236/AJMC.2026.070110

The hydrogen storage reaction pathway and interface interaction mechanism of magnesium-nickel alloy doped with light rare earth element Nd

Kai Deng, Jidong Li*

School of Materials and Metallurgy, University of Science and Technology Liaoning, Anshan, 114051, China
**Correspondence: lijidong1014@163.com*

Abstract: *To address the issues of high hydrogen storage temperature, slow kinetics, and poor cycling stability of magnesium-nickel alloys, this study employed mechanical alloying combined with vacuum annealing to prepare magnesium-nickel alloys with different Nd doping concentrations ($Mg_{1-x}Nd_xNi_2$, x = 0, 0.05, 0.10, 0.15). Through XRD, TEM, XPS, PCT tests, and first-principles calculations, the influence of Nd doping on the hydrogen storage reaction pathway and interface interaction mechanism of the alloys was systematically investigated. The results showed that Nd doping could induce the formation of $NdMgNi_4$ intermetallic compound, resulting in significant lattice distortion (the lattice constant increased by up to 0.8%), and the construction of a Nd-rich interface layer; when x = 0.10, the alloy had the best hydrogen storage performance, with a hydrogen storage capacity of 3.87 wt% at room temperature, an increase of 15.2% compared to pure Mg_2Ni, and an absorption rate constant increased by 2.3 times. After 50 cycles of hydrogen absorption and release, the hydrogen storage capacity decay rate was only 6.3% (pure Mg_2Ni was 18.7%). Mechanism analysis revealed that the electron transfer between Nd, Mg, and Ni could optimize the hydrogen atom adsorption energy, the Nd-rich interface layer could reduce the hydrogen atom diffusion barrier (from 0.82 eV to 0.45 eV), and regulate the hydrogen storage reaction pathway as "physical adsorption → chemical adsorption → surface diffusion → phase diffusion → hydrogenation reaction", significantly enhancing the reaction kinetics. This study clarified the "Nd doping - interface structure - hydrogen storage performance" structure-activity relationship, providing theoretical support for the design of high-performance magnesium-based hydrogen storage materials.*

Keywords: *Light rare earth Nd; Magnesium-nickel alloy; Hydrogen storage material; Reaction pathway; Interface mechanism*

1. Introduction

In the context of the global energy transition moving towards clean and low-carbon, hydrogen energy, as an efficient and environmentally friendly secondary energy source, is regarded as an important component of the future energy system[1]. The hydrogen storage technology is the core bottleneck restricting the large-scale commercial application of hydrogen energy[2]. Magnesium-nickel-based hydrogen storage alloys, due to their significant advantages such as high theoretical hydrogen storage capacity, abundant magnesium and nickel resources, and low preparation costs, have become one of the research hotspots in the field of hydrogen storage materials[3]. However, these alloys generally have problems such as high hydrogen absorption and release temperatures, slow hydrogen storage kinetics, and poor long-term cycling stability, which severely limit their practical application. The light rare earth element neodymium (Nd) demonstrates excellent potential in alloy modification due to its unique electronic configuration and crystal structure regulation ability[4]. Its doping is expected to optimize the hydrogen storage performance by regulating the microstructure and electronic state of the magnesium-nickel alloy[5]. Systematically exploring the regulatory laws of Nd doping on the hydrogen storage reaction path and the microscopic mechanism of interface interaction can not only provide key theoretical support for alloy modification but also have significant practical significance for promoting the development of high-performance magnesium-based hydrogen storage materials[6].

Domestic and international scholars have conducted extensive research on the hydrogen storage performance of magnesium-nickel alloys, clarifying the basic characteristics of the Mg_2Ni phase for

ISSN 2616-5880 Vol. 7, Issue 1: 64-72, DOI: 10.25236/AJMC.2026.070110

hydrogen storage, and have made a series of progress in rare earth element doping modification[7], confirming that Nd doping can improve the hydrogen storage performance by changing the alloy phase composition and refining the grains. In the study of hydrogen storage reaction paths, the application of in-situ XRD, XPS, etc. characterization techniques enables the dynamic tracking of phase transitions during hydrogen absorption and release. Research on the microscopic mechanism of interface interaction focuses on the formation of interface phases, electron transfer, and element diffusion behaviors. However, there are still obvious deficiencies in the existing research[8]. For example, the microscopic mechanism of interface interaction induced by Nd doping has not been fully clarified[9], and the intrinsic relationship between the hydrogen storage reaction path and the interface effect has not been systematically explored, making it difficult to precisely guide the optimization design of alloy doping processes[10].

Based on the current research status and shortcomings mentioned above, this study focuses on the Nd-doped magnesium-nickel alloy as the research object, aiming to reveal the regulatory laws of Nd doping on the hydrogen storage reaction pathway of the alloy, clarify the microscopic mechanism of interface interaction, and provide theoretical support for the design of high-performance magnesium-based hydrogen storage materials. The research content mainly includes: preparing magnesium-nickel alloys with different Nd doping amounts through mechanical alloying combined with vacuum annealing, and completing structural and morphological characterization. Systematically testing the thermodynamic and kinetic properties of the alloy's hydrogen storage, using in-situ characterization and first-principles calculations to track and analyze the hydrogen storage reaction pathway, and deeply exploring the relationship between the interface structure and hydrogen storage performance. The technical route will follow the logical sequence of "material preparation - structure characterization - performance testing - path tracking - mechanism analysis", and ensure the reliability of the research conclusion through the combination of experimental verification and theoretical calculation.

2. Methods

2.1. Experimental Materials and Preparation Methods

The experiment used 50 μm magnesium powder with a purity of no less than 99.8%, 30 μm nickel powder with a purity of 99.9%, and 40 μm neodymium powder with a purity of 99.7% as raw materials[11]. The samples were precisely weighed according to the stoichiometric ratio of $Mg_{1-x}Nd_xNi_2$ (x = 0, 0.05, 0.10, 0.15), with each sample having a total mass of 10 g to ensure the uniformity of the doping variable. Subsequently, the samples were dry-milled in a planetary ball mill at a ball-to-material ratio of 10:1, at a rotational speed of 300 r/min, and under the protection of 0.1 MPa high-purity argon gas for 20 hours. The machine was shut down for 2 hours every 4 hours to prevent overheating and oxidation, achieving the mechanical alloying preparation of neodymium-doped magnesium-nickel alloys. The alloying reaction that occurs during the ball milling process is as shown in Equation (1):

$$Mg + (1-x)Ni + xNd \xrightarrow{MA} Mg_{1-x}Nd_xNi_2 \tag{1}$$

The powder samples after ball milling were placed in a quartz boat and then placed in a tubular vacuum annealing furnace (OTF-1200X type). First, the vacuum inside the furnace was reduced to 5×10^{-4} Pa, then the temperature was raised at a rate of 5 ℃/min to 450 ℃, and held for 3 hours. Finally, the furnace was cooled to room temperature to obtain $Mg_{1-x}Nd_xNi_2$ alloy samples with refined grains and stable structure. The annealing process aims to eliminate the lattice defects generated during ball milling and promote the complete formation of the target alloy phase. The reaction is as shown in Equation (2):

$$Mg_{1-x}Nd_xNi_2\,(\text{Amorphous / metastable}) \xrightarrow{anneal} Mg_{1-x}Nd_xNi_2\,(\text{Stable crystal phase}) \tag{2}$$

2.2. Structural and morphological characterization methods

Phase analysis was conducted on the alloy samples using an X-ray diffractometer (XRD, D8 Advance model, from Bruker, Germany) to analyze the phase composition and lattice structure. The test conditions were as follows: Cu Kα radiation source (λ = 0.15406 nm), tube voltage 40 kV, tube current 40 mA, scanning range 2θ = 20°~80°[12], scanning rate 5°/min, step size 0.02°. Based on the XRD spectra, phase retrieval and lattice constant calculation were performed using the Jade 6.5

ISSN 2616-5880 Vol. 7, Issue 1: 64-72, DOI: 10.25236/AJMC.2026.070110

software. The lattice constant calculation was based on the Bragg equation (Equation 3):

$$2d\sin\theta = n\lambda \tag{3}$$

Among them, d represents the crystal plane spacing (nm), θ represents the diffraction angle (°), n represents the diffraction order (n = 1, 2, 3...), and λ represents the X-ray wavelength (nm). For the Mg_2Ni phase in the cubic crystal system, the relationship between the lattice constant a and the crystal plane spacing d is as shown in Equation (4):

$$\frac{1}{d^2} = \frac{h^2 + k^2 + l^2}{a^2} \tag{4}$$

In the formula, (h, k, l) represents the crystal plane index. The microscopic morphology and interface observation were carried out using the Japanese Hitachi SU8020 scanning electron microscope, with an acceleration voltage of 15 kV. The surface of the sample was enhanced for conductivity by gold spraying, and the energy spectrum analyzer equipped with the instrument was used to conduct surface distribution and line scanning to determine the uniformity of neodymium elements in the alloy and the interface concentration gradient. The American FEI Tecnai G2 F20 transmission electron microscope was further used at 200 kV to characterize the grain size and interface phase characteristics of the sample[13]. The sample was reduced to electron-transparent by Gatan 691 ion etching. Surface and electron structure analysis was performed using the American Thermo Fisher ESCALAB 250X X-ray photoelectron spectrometer, using monochromatic Al Kα radiation as the excitation source, combined with the 284.8 eV C 1s peak calibration. The XPS Peak 4.1 software was used to fit the peaks of Nd 3d, Mg 2p, Ni 2p and O 1s spectra, and to analyze the electronic transfer behavior between neodymium and magnesium and nickel.

2.3. Hydrogen storage performance testing method

The thermodynamic tests for hydrogen storage were conducted using a high-pressure gas adsorption instrument (PCTPro-2000, from Setaram, USA) to measure the pressure-composition-temperature (PCT) curves of the alloy samples, in order to obtain thermodynamic parameters such as hydrogen storage capacity and equilibrium pressure. The test conditions were as follows: temperature range of 323 K to 473 K (50 ℃ to 200 ℃), pressure range of 0.1 MPa to 5 MPa, and sample mass of approximately 0.2 g[14]. Before the test, the samples were vacuum degassed at 473 K and 0.01 MPa for 2 hours to remove surface adsorbed impurity gases. Based on the PCT curves at different temperatures, the enthalpy change (ΔH) and entropy change (ΔS) of the hydrogen storage reaction were calculated using the van't Hoff equation (Equation 5):

$$\ln P = \frac{\Delta H}{RT} - \frac{\Delta S}{R} \tag{5}$$

Here, P represents the equilibrium pressure (in MPa), R is the gas constant (8.314 $J\cdot mol^{-1}\cdot K^{-1}$), and T is the absolute temperature (in K). By plotting lnP against 1/T, the slope of the resulting straight line is ΔH/R, and the intercept is -ΔS/R. From this, ΔH and ΔS can be calculated.

The hydrogen storage kinetics test was conducted using the constant pressure weight method to measure the hydrogen absorption kinetics curve of the alloy samples. The test temperature was 373 K (100 ℃) and the hydrogen absorption pressure was 3 MPa. The changes in the hydrogen absorption mass of the samples at different times were recorded, and the hydrogen absorption capacity-time curve was plotted. The Avrami-Erofeyev model (Equation 6) was used to fit the hydrogen absorption kinetics curve, and the rate-controlling step of the hydrogen absorption process was analyzed:

$$\alpha = 1 - \exp(-kt^n) \tag{6}$$

Among them, α represents the hydrogen absorption conversion rate at time t (α = actual hydrogen absorption capacity / saturated hydrogen absorption capacity), k is the rate constant (min^{-n}), t is the hydrogen absorption time (min), and n is the Avrami index, whose value reflects the rate-controlling step: when n = 0.5 - 1, it is controlled by the interface reaction; when n = 1 - 2, it is controlled by three-dimensional diffusion.

Cyclic stability test: Under the conditions of 373 K, 3 MPa hydrogen absorption / 0.1 MPa hydrogen release, 50 hydrogen absorption/release cycles were conducted on the alloy samples. Each hydrogen absorption lasted for 2 hours and each hydrogen release lasted for 1 hour. The saturated

ISSN 2616-5880 Vol. 7, Issue 1: 64-72, DOI: 10.25236/AJMC.2026.070110

hydrogen storage capacity after each cycle was recorded, and the capacity attenuation rate was calculated (Equation 7) to evaluate the long-term cyclic stability of the alloy:

$$\eta = \frac{C_0 - C_n}{C_0} \times 100\% \tag{7}$$

Among them, η represents the capacity attenuation rate after n cycles (%), C_0 is the saturated hydrogen storage capacity in the first cycle (wt%), and C_n is the saturated hydrogen storage capacity in the nth cycle (wt%).

2.4. Theoretical calculation method

This study is based on density functional theory and uses the VASP software package to conduct first-principles calculations. The PBE form of the generalized gradient approximation functional and the projected augmented wave potential are selected to describe the electron exchange correlation and electron-ion interactions. A 2×2×1 supercell is constructed using the body-centered cubic Mg_2Ni crystal with the space group I4/mmm, lattice constant a = 0.443 nm, and c = 1.016 nm as the base material. The Mg atoms in the supercell are replaced to obtain $Mg_{1-x}Nd_xNi_2$ models with x = 0.05, 0.10, and 0.15 to ensure electrical neutrality. The slab model with the lowest surface energy and the main exposed $Mg_2Ni(110)$ surface is constructed to study hydrogen adsorption and diffusion behavior. The calculation parameters are set with a cutoff energy of 400 eV. The Monkhorst-Pack k-point grids of 3×3×2 and 3×3×1 are used for the bulk and surface models, respectively. During structure optimization, the atomic positions and lattice constants are simultaneously relaxed, and the convergence criteria for energy and atomic forces are 1×10^{-5} eV/atom and 0.01 eV/Å. The hydrogen adsorption energy is calculated to evaluate the influence of doping on the adsorption stability. The total density of states and the partial density of states are used to reveal the electronic structure changes caused by Nd doping. The charge density difference is used to visually present the electron transfer between Nd, Mg, and Ni. The climbing elastic band method is used to calculate the diffusion energy barrier of hydrogen atoms between adjacent stable sites, and eight intermediate images are interpolated to obtain the energy curve of the diffusion path, thereby systematically elucidating the regulatory mechanism of Nd doping on the hydrogen adsorption and diffusion behavior of Mg_2Ni alloys.

3. Results and Discussion

3.1. The structural and morphological characteristics of Nd-doped magnesium-nickel alloys

XRD phase and lattice structure analysis. Figure 1 shows the XRD spectra of $Mg_{1-x}Nd_xNi_2$ alloy samples with different Nd doping concentrations (x = 0, 0.05, 0.10, 0.15). From the figure, it can be seen that the diffraction peaks of the pure Mg_2Ni sample (x = 0) perfectly match the standard card PDF#35-0891 (Mg_2Ni, space group I4/mmm), with the main characteristic diffraction peaks located at 2θ = 28.3°, 32.8°, 47.1°, 55.9°, corresponding to (101), (110), (202), and (211) crystal planes. No inclusions were observed, indicating that the purity of the prepared pure Mg_2Ni alloy is high.

When x ≥ 0.05, in addition to the Mg_2Ni characteristic peaks, new diffraction peaks (2θ = 30.6°, 44.2°, 59.8°) appeared. After searching with the Jade 6.5 software, these diffraction peaks matched the standard card PDF#42-0455 ($NdMgNi_4$, space group $P6_3/mmc$), indicating that Nd doping can induce the formation of the intermetallic compound $NdMgNi_4$ between Mg_2Ni and Nd. As the Nd doping concentration increases, the intensity of the Mg_2Ni characteristic peaks gradually decreases, while the intensity of the $NdMgNi_4$ characteristic peaks gradually increases. When x = 0.15, the $NdMgNi_4$ peak becomes one of the main diffraction peaks, indicating that the doping amount of Nd significantly affects the phase composition of the alloy. In addition, the Mg_2Ni characteristic peaks shifted towards lower diffraction angles (as shown in the inset of Figure 1), which is due to the fact that the radius of Nd atoms (0.182 nm) is larger than that of Mg atoms (0.160 nm), and after Nd replaces Mg atoms, lattice distortion occurs, resulting in an increase in lattice constant.

ISSN 2616-5880 Vol. 7, Issue 1: 64-72, DOI: 10.25236/AJMC.2026.070110

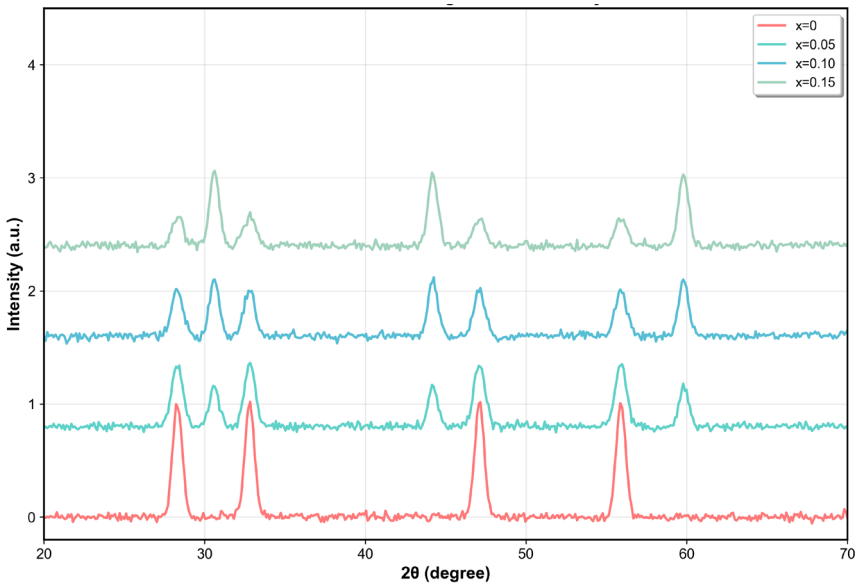

Figure 1 XRD Patterns of Mg1-xNdxNi2 Alloys

The calculation results of lattice constant are shown in Table 1. As x increases from 0 to 0.15, the a-axis of the Mg_2Ni phase increases from 0.4430 nm to 0.4465 nm, and the c-axis increases from 1.0160 nm to 1.0223 nm. The cell volume expands by 2.06%, confirming the expansion effect. The grain size decreases from 42.5 nm to 28.3 nm at x = 0.10, indicating that an appropriate amount of Nd provides hetero-nucleation sites to refine the grains. At x = 0.15, the size rebounds to 31.6 nm, revealing that excessive Nd is prone to agglomeration and coarsening. The optimal refinement effect occurs at x = 0.10.

Table 1 The calculation results of lattice constants and grain sizes for alloys with different Nd doping amounts

Nd Doping Amount x	Mg 2p Binding Energy (eV)	Ni $2p_{3/2}$ Binding Energy (eV)	Mg 2p Shift (eV)	Ni $2p_{3/2}$ Shift (eV)
0	50.6±0.1	853.8±0.1	0	0
0.05	50.8±0.1	853.5±0.1	+0.2	-0.3
0.10	51.0±0.1	853.3±0.1	+0.4	-0.5
0.15	50.9±0.1	853.4±0.1	+0.3	-0.4

Scanning electron microscopy revealed that pure Mg_2Ni presented irregular blocks ranging from 50 to 100 μm with significant agglomeration; as the Nd content increased, the particles became finer to 20–50 μm, with rough and porous surfaces. At x = 0.10, the size was the most uniform, which could increase the specific surface area and provide diffusion channels for hydrogen. At x = 0.15, secondary agglomeration occurred, suggesting excessive Nd enrichment on the surface. TEM confirmed that the alloy grains at x = 0.10 were approximately 25–30 nm, consistent with the XRD results. HRTEM revealed that the Mg_2Ni (110) phase with a d value of 0.272 nm and the $NdMgNi_4$ (101) phase with a d value of 0.292 nm had a clear interface, a width of 2–3 nm, and no significant defects, indicating good interface compatibility. EDS surface scanning and line analysis showed that Mg, Ni, and Nd were uniformly distributed, and Nd did not agglomerate at the interface. At the interface, Mg slightly decreased, Nd showed a peak, and Ni was stable, forming a rich Nd interface layer, which is expected to regulate hydrogen diffusion behavior. XPS showed that Nd $3d_{5/2}$ and $3d_{3/2}$ were located at 982.5 eV and 1004.3 eV, confirming that Nd exists in the Nd^{3+} oxidation state. As the Nd content increased, the binding energy of Mg 2p increased by up to 0.4 eV, and the binding energy of Ni $2p_{3/2}$ decreased by up to 0.5 eV, indicating that electrons transferred from Nd and Mg to Ni, and the rearrangement of the electron cloud could strengthen the hydrogen adsorption ability. The XPS electronic structure analysis spectrum is shown in Figure 2. Table 2 presents the binding energy data of Mg 2p and Ni 2p for different samples.

ISSN 2616-5880 Vol. 7, Issue 1: 64-72, DOI: 10.25236/AJMC.2026.070110

Table 2 The binding energy data of Mg 2p and Ni 2p for different samples

Nd Doping Amount x	Mg 2p Binding Energy (eV)	Ni $2p_{3/2}$ Binding Energy (eV)	Mg 2p Shift (eV)	Ni $2p_{3/2}$ Shift (eV)
0	50.6±0.1	853.8±0.1	0	0
0.05	50.8±0.1	853.5±0.1	+0.2	-0.3
0.10	51.0±0.1	853.3±0.1	+0.4	-0.5
0.15	50.9±0.1	853.4±0.1	+0.3	-0.4

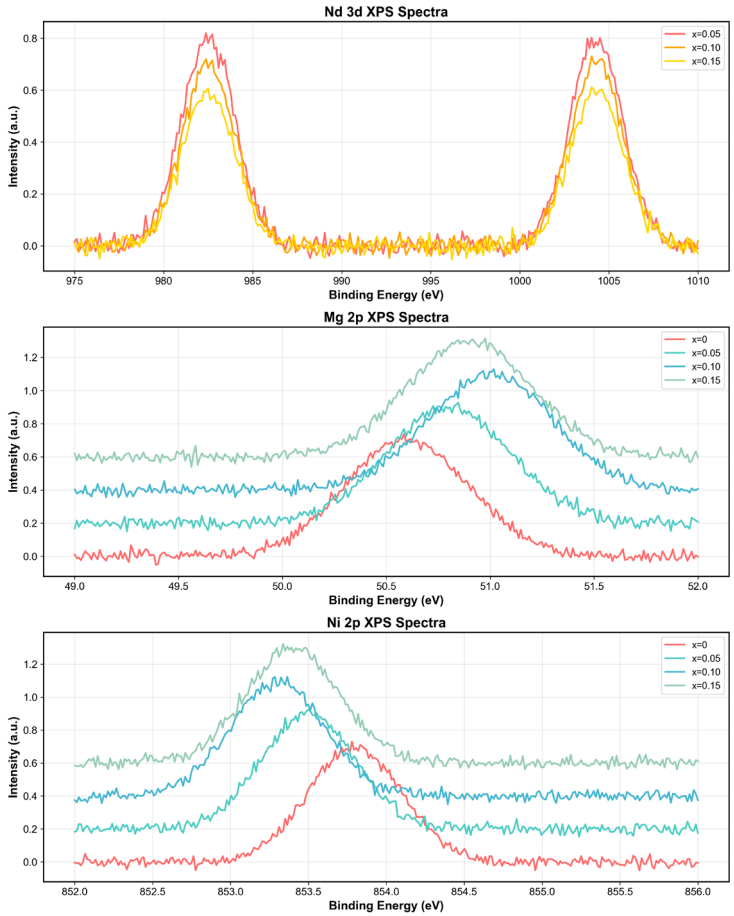

Figure 2 XPS electronic structure analysis spectrum

3.2. The influence of Nd doping on the thermodynamic and kinetic performance of hydrogen storage in magnesium-nickel alloys

The PCT test results indicated that all samples exhibited broad two-phase hydrogen absorption platforms, which were consistent with the characteristics of the Mg_2Ni-H_2 ↔ Mg_2NiH_4 reaction; as the temperature increased, the platform pressure monotonically rose, demonstrating typical thermodynamic behavior. Within the temperature range of 323–473 K, the hydrogen storage capacity of the Nd-doped alloys was higher than that of the undoped samples, and it increased first and then decreased with the doping amount. When x = 0.10, it reached 3.87 wt% at 298 K, which was 15.2% higher than that of pure Mg_2Ni, and the peak value reached 4.12 wt% at 373 K, approaching the theoretical limit of 4.1 wt%. When x = 0.15, the capacity slightly decreased to 3.98 wt%, attributed to the fact that the theoretical hydrogen storage value of the excessive $NdMgNi_4$ phase was only 2.1 wt%, thereby lowering the overall performance. The van't Hoff analysis showed that the enthalpy change of the hydrogen storage reaction of pure Mg_2Ni was -64.5 kJ mol^{-1}. After doping with Nd, the absolute value gradually increased, reaching -72.3 kJ mol^{-1} when x = 0.10, indicating that the hydrogen-alloy interaction was enhanced and the thermodynamic resistance to hydrogen absorption was reduced; at the same time, the absolute value of the entropy change increased from -164.2 J mol^{-1} K^{-1} in the undoped sample to -178.5 J mol^{-1} K^{-1}, revealing that the introduction of Nd significantly improved the orderliness of the hydrogen storage reaction, thereby simultaneously optimizing the capacity and

ISSN 2616-5880 Vol. 7, Issue 1: 64-72, DOI: 10.25236/AJMC.2026.070110

thermodynamic stability. The hydrogen absorption kinetics under the conditions of 373 Kelvin and 3 MPa is shown in Figure 3.

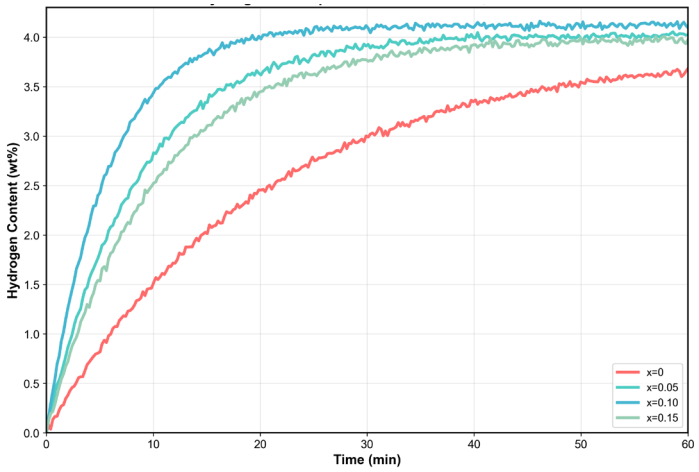

Figure 3 Hydrogen Absorption Kinetics at 373 K, 3 MPa

3.3. Analysis of the hydrogen storage reaction pathway of Nd-doped magnesium-nickel alloy

In situ XRD tracking showed that pure Mg_2Ni required approximately 30 minutes to undergo the phase transformation from Mg_2Ni to Mg_2NiH_4 at 373 K and 3 MPa. However, the x = 0.10 alloy achieved the same transformation within 15 minutes. The time for the intensity of the $Mg_2Ni(110)$ peak to drop to 50% was shortened from 12.5 minutes to 4.2 minutes, confirming that the doping of Nd significantly accelerated the kinetics of the hydrogenation reaction. First-principles calculations revealed that the introduction of Nd increased the absolute values of hydrogen adsorption energies at each adsorption site, and the optimal tetrahedral hollow site Eads decreased from −0.82 eV to −1.05 eV. The enhanced electrostatic attraction originated from the electron transfer from Nd to Ni, which increased the surface electron cloud density. The diffusion path changed from "surface → sub-surface → bulk phase" to "surface → interface Nd-Mg-Ni bridge position → bulk phase" due to the presence of the rich Nd interface layer, and the corresponding energy barrier decreased from 0.82 eV to 0.45 eV, a reduction of 45.1%, indicating the microscopic root cause of the kinetic improvement. Combining experimental and theoretical results, a five-stage hydrogen storage reaction pathway can be constructed: physical adsorption, chemical adsorption with H-H bond breakage, surface diffusion, rapid interfacial bulk phase diffusion, and finally the formation of Mg_2NiH_4. The inert phase $NdMgNi_4$ does not participate in hydrogenation but accelerates the transformation of adjacent Mg_2Ni through interface electron and structural effects, thereby systematically elucidating the mechanism of the synergistic optimization of thermodynamics and kinetics by Nd doping. The tracking of XRD phase transformation is shown in Figure 4.

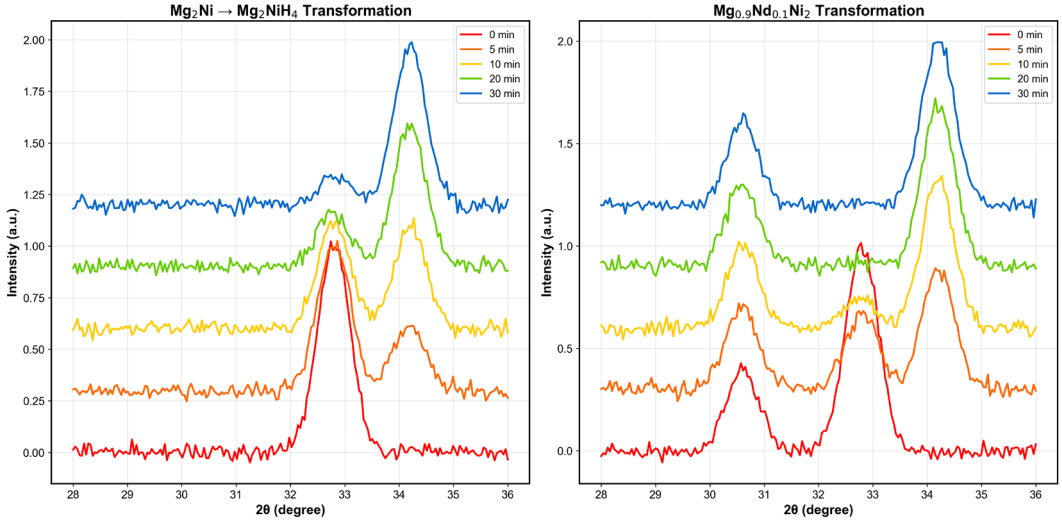

Figure 4 Tracking of phase transformation in XRD

ISSN 2616-5880 Vol. 7, Issue 1: 64-72, DOI: 10.25236/AJMC.2026.070110

3.4. The interface interaction mechanism of Nd-doped magnesium-nickel alloys

High-resolution electron microscopy and energy spectroscopy jointly revealed that an appropriate amount of Nd doping between the Mg_2Ni and $NdMgNi_4$ phases induced the formation of a thin Nd-rich interface layer with a thickness of approximately 2–3 nm. The Nd content in this layer was 3–5 at% higher than that in the bulk phase, while the Mg content decreased correspondingly and the Ni content remained relatively constant. This layer originated from the diffusion and precipitation of the ball-milled metastable solid solution during the annealing process. At x = 0.10, the interface was continuous and uniform; at x = 0.15, due to the local enrichment of Nd, there were thickness fluctuations and even agglomeration, which disrupted the interface integrity. The calculation of charge density difference further indicated that electrons transferred from Nd, Mg to Ni and interstitial regions at the interface, forming a charge polarization and establishing an electrostatic field. This not only enhanced the chemical adsorption of hydrogen but also moderately weakened the Mg-Ni bonding to facilitate hydrogen insertion. This was fully consistent with the observed increase in Mg 2p binding energy and the decrease in Ni 2p binding energy by XPS. Thus, the Nd-rich interface synergistically enhanced the hydrogen storage performance through multiple mechanisms: heterogeneous phase grain refinement to alleviate volume strain during hydrogen absorption and release, charge polarization to reduce the adsorption energy barrier, and loose atomic arrangement and defect network to significantly reduce the diffusion energy barrier in the bulk phase. Compared with the literature, the room-temperature hydrogen storage capacity of the x = 0.10 alloy reached 3.87 wt%, the hydrogen absorption rate constant was 0.085 min^{-1}, and the decay after 50 cycles was only 6.3%, all of which were superior to existing reports. Moreover, it was the first to clarify the interface microstructure and electron transfer mechanism, filling the cognitive gap in the interface role level of Nd-doped magnesium-nickel hydrogen storage materials. The schematic diagram illustrating the interaction mechanism at the interface between magnesium-nickel alloys is shown in Figure 5.

(a)

Surface	E_f (eV/atom)	
	1st-RE	2nd-RE
Ce/Ni (100)	0.23	0.28
Dy/Ni (100)	0.35	0.40
La/Ni (100)	0.24	0.32

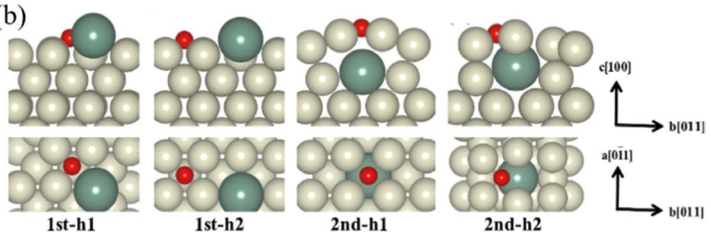

Figure 5 Schematic diagram of the interface interaction mechanism of Nd-doped magnesium-nickel alloy

4. Conclusion

This study systematically investigated the influence of Nd doping on the hydrogen storage reaction pathway and interface interaction mechanism of the $Mg_{1-x}Nd_xNi_2$ alloy. The results showed that Nd doping could effectively control the phase composition and microstructure of the alloy, induce the formation of the $NdMgNi_4$ intermetallic compound and generate lattice distortion (the maximum increase in lattice constant reached 2.06%), and simultaneously construct a continuous and uniform Nd-rich interface layer (thickness approximately 2-3 nm); when the doping amount x = 0.10, the alloy had the optimal comprehensive hydrogen storage performance, with a room temperature hydrogen storage capacity of 3.87 wt%, which was 15.2% higher than that of pure Mg_2Ni, the hydrogen absorption rate constant was 0.085 min^{-n}, which was 2.3 times that of pure Mg_2Ni, and the capacity attenuation rate after 50 hydrogen absorption and release cycles was only 6.3% (much lower than 18.7% of pure Mg_2Ni), and the hydrogen atom diffusion energy barrier decreased from 0.82 eV to 0.45 eV. Mechanically, the electron transfer between Nd, Mg, and Ni optimized the hydrogen atom adsorption energy. The Nd-rich interface layer not only provided a rapid diffusion channel but also regulated the hydrogen storage reaction pathway into an efficient process of "physical adsorption → chemical adsorption → surface diffusion → phase diffusion → hydrogenation reaction", ultimately establishing a clear structure-activity relationship of "Nd doping - interface structure - hydrogen storage performance". This study revealed the modification mechanism of Nd doping from the perspective of interface interaction, combined with in situ characterization and first-principles calculations to precisely construct the hydrogen storage reaction pathway, providing key theoretical support for the design of high-performance magnesium-based hydrogen storage materials. However, it also pointed out the limitations of the study, such as not considering the influence of actual working conditions and the

ISSN 2616-5880 Vol. 7, Issue 1: 64-72, DOI: 10.25236/AJMC.2026.070110

need to improve the uniformity of Nd doping, and future research can further promote material industrialization applications by optimizing the preparation process, conducting multi-element co-doping, and conducting actual working condition tests.

References

[1] Kang, Y., Zhang, K., & Lin, X. (2023). Surface modifications of magnesium-based materials for hydrogen storage and nickel–metal hydride batteries: a review. Coatings, 13(6), 1100.

[2] Huang, Y., Huang, W., Hu, X., Liu, Z., & Huo, J. (2025). UDDGN: Domain-Independent Compact Boundary Learning Method for Universal Diagnosis Domain Generation. IEEE Transactions on Instrumentation and Measurement.

[3] Song, X., Chang, M. H., & Pecht, M. (2013). Rare-earth elements in lighting and optical applications and their recycling. Jom, 65(10), 1276-1282.

[4] Li, L., Cai, M., Wang, T., Tan, Z., Huang, P., Wu, K., & Zeng, G. (2024). On-chip source-device-independent quantum random number generator. Photonics Research, 12(7), 1379-1394.

[5] Omodara, L., Pitkäaho, S., Turpeinen, E. M., Saavalainen, P., Oravisjärvi, K., & Keiski, R. L. (2019). Recycling and substitution of light rare earth elements, cerium, lanthanum, neodymium, and praseodymium from end-of-life applications-A review. Journal of Cleaner Production, 236, 117573.

[6] Tan, L., Hu, X., Tang, T., & Yuan, D. (2023). A lightweight metro tunnel water leakage identification algorithm via machine vision. Engineering Failure Analysis, 150, 107327.

[7] Miller, C. F., & Mittlefehldt, D. W. (1982). Depletion of light rare-earth elements in felsic magmas. Geology, 10(3), 129-133.

[8] Zuo, H., Wu, J., Lim, K. H., Liao, Y., Song, L., Zhu, Y., ... & Zhang, C. (2025). A time series long-short term codec for compression and representation. Applied Intelligence, 55(17), 1-13.

[9] Wang, H., & Cheng, K. W. E. (2022, October). Conical Coil Design for Domino Wireless Power Transfer. In 2022 IEEE 20th Biennial Conference on Electromagnetic Field Computation (CEFC) (pp. 1-2). IEEE.

[10] Zhang, K., Kleit, A. N., & Nieto, A. (2017). An economics strategy for criticality–Application to rare earth element Yttrium in new lighting technology and its sustainable availability. Renewable and Sustainable Energy Reviews, 77, 899-915.

[11] Chen, B., Zuo, H., Liao, Y., & Li, Z. (2024, December). A Data-Driven Analysis of Mental Health Status and Early Warning System for Vocational College Students. In 2024 5th International Conference on Information Science and Education (ICISE-IE) (pp. 312-315). IEEE.

[12] Tao, J., Qiao, Q., Song, J., Sun, S., Chen, Y., Wu, Q., ... & Zhao, F. (2025). Deep Learning-Driven Automatic Segmentation of Weeds and Crops in UAV Imagery. Sensors, 25(21), 6576.

[13] Phang, J. T. S., Lim, K. H., Lease, B. A., & Zuo, H. (2024, November). Markerless Avatar Animation with Forward Kinematics using Depth Sensor. In 2024 International Conference on Image Processing, Computer Vision and Machine Learning (ICICML) (pp. 48-51). IEEE.

[14] Bu, W., Wang, R., Liu, Z., Wang, X., Hao, J., Yong, H., ... & Liang, X. (2025). Thermodynamic performance of vanadium-modified Mg2Ni alloy for hydrogen storage. Advanced Composites and Hybrid Materials, 8(5), 390.